THE JOURNAL OF PHYSICAL CHEMISTRY C

Article

pubs.acs.org/JPCC

Impacts of Reduced Graphene Oxide in CdS/CdSe Quantum Dots Co-sensitized Solar Cells

Qiang Wu,[†,‡] Haifeng Zhao,[†,‡] Fei Huang,[§] Juan Hou,*[,†,‡] Haibin Cao,[†] Zhiyong Liu,[‡] Shanglong Peng,[§] and Guozhong Cao*[,§]

[†]College of Science/Key Laboratory of Ecophysics and Department of Physics, [‡]School of Chemistry and Chemical Engineering/Key Laboratory for Green Process of Chemical Engineering of Xinjiang Bingtuan, Shihezi University, Xinjiang Shihezi 832003, P. R. China

[§]Department of Materials and Engineering, University of Washington, Seattle, Washington 98195-2120, United States

Supporting Information

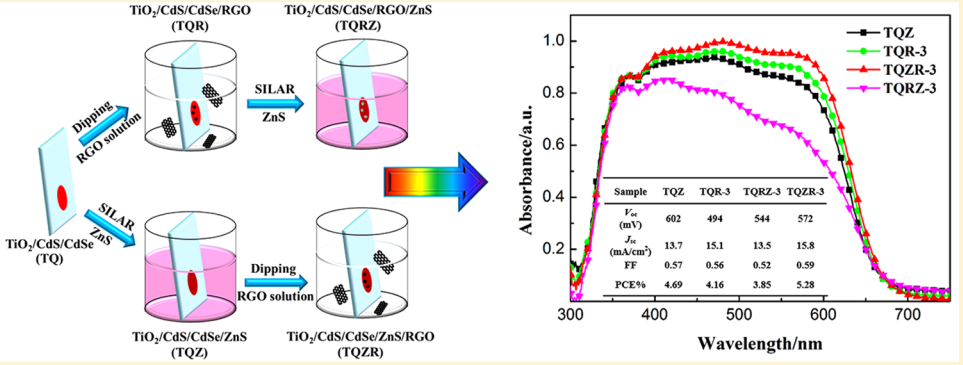

ABSTRACT: The introduction of various amounts of reduced graphene oxide (RGO) to CdS/CdSe quantum dots co-sensitized solar cells was investigated to enhance the light absorption and to promote the electron transfer. The characterization and comparison of optical and electrochemical properties as well as the performance of the resultant quantum dot-sensitized solar cells (QDSCs) with different amounts of RGO have been investigated systematically. The introduction of RGO demonstrated to enhance the light harvesting and consequently increase the short-circuit current density (J_{sc}). ZnS inserting between QDs and RGO can effectively block the charge recombination at the interface; however, the defects of RGO in the TiO_2/QDs/ZnS/RGO photoanode still may accelerate the interface charge recombination in QDSCs and lead to a slight decrease of the open-circuit voltage (V_{oc}). The balance between the light harvesting and charge recombination in RGO modified QDSCs is a key for achieving high power conversion efficiency (PCE). Finally, the CdS/CdSe/ZnS co-sensitized cell with modification RGO (3 min) achieved a high PCE of 5.28% (J_{sc} = 15.8 mA/cm^2, V_{oc} = 572 mV), more than 13% higher than that of 4.69% (J_{sc} = 13.7 mA/cm^2, V_{oc} = 602 mV) obtained for the cell without RGO.

1. INTRODUCTION

As one of the third generation solar cells, quantum dot-sensitized solar cells (QDSCs) have received wide academic and commercial interest and mainly benefit from superior properties of quantum dots including high stability, large extinction coefficients, and tunable band gap across, large intrinsic dipole moment as well as solution processability.[1−3] Moreover, the theoretical power conversion efficiency (PCE) of QDSCs can be reached as high as 44% in consideration of the hot electron extraction and multiple exciton generation (MEG) effect.[4,5] At present, the highest PCE of QDSCs sensitized with CuZnInSe QDs is 11.6%,[6] which is still lower than that of the dye-sensitized solar cells (13.0%)[7] and perovskite solar cells (22.1%).[8] Great progresses have been made in improving the PCE of QDSCs in the past few years by optimizing the components constituting the device, such as the modification of the photoanode,[9] improving the electrocatalytic activity of the counter electrode,[10] and the configuration of sensitizers.[11] Considerable studies have been performed on narrow band gap semiconductor QDs including CdS,[12] CdSe,[13] CdS_xSe_{1-x},[11] CdSeTe,[14] CuInS,[15] and CuZnInSe.[6] CdS/CdSe QDs selected as co-sensitizer for QDSCs have been the most frequently studied due to their broad light absorption, effective charge injection, and easy synthesis.[16−19] However, the relatively lower harvesting efficiency was a primarily factor which influences the performance of QDSCs. Considerable methods have been attempted to enhance the light harvesting capability, such as optimization of photoanode structure to increase the QDs loading amount,[20] introduction of transition metal ions into QDs to tune the range of light absorption,[21] and utilization of

Received: June 24, 2017
Revised: August 4, 2017
Published: August 7, 2017

DOI: 10.1021/acs.jpcc.7b06192
J. Phys. Chem. C 2017, 121, 18430−18438

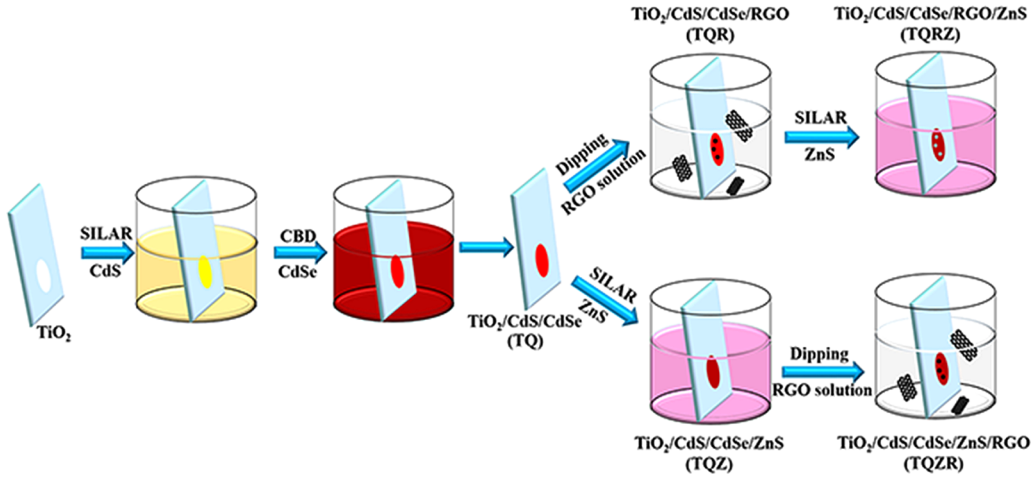

Figure 1. Schematic illustration of the fabrication process of the photoanodes sensitized with QDs and deposited ZnS and RGO in different sequence.

light scattering effect to improve optical absorption.[22] Cheng et al. have succeeded in employing Ag plasmonic nanoparticles as "scatterers" on the surface of a photoanode, resulting in a significant increase in the light harvesting capability and yielded the PCE of 1.73%.[22] A literature review reported that the wrinkle structure of graphene also exhibits a light scattering effect which can further increase the absorption of Al nanoparticle-enhanced solar cells, and thus a 7.2% enhancement in the short-circuit current density (J_{sc}) can be achieved through the integration of plasmonic Al nanoparticles and wrinkle-like graphene sheets.[23]

Recently, graphene and graphene-based semiconductor composites have attracted a lot of attention because of their promising potential for conversion of solar energy. As a two-dimensional (2D) honeycomb carbon sheet, graphene is made of carbon atoms with a single atomic layer connected by sp_2 hybridization; the basic structural unit was the most stable benzene ring.[24] It is well-known that the unique structure of graphene lead to many excellent performances, such as huge specific surface area, high mechanical properties, superior electronic mobility, and remarkable optical transmittance.[25] On the basis of these merits, graphene and graphene-based semiconductor nanocomposites are regarded as the electron reservoir to capture/shuttle the electrons photogenerated from the semiconductor. For example, Deng et al. demonstrated that incorporation of graphene in ZnO nanorods can help to facilitate electron transfer and suppress the interfacial carrier recombination, leading to improved efficiency.[26] Kamat et al. employed the Cu_2S-RGO composite as the counter electrode and succeeded in shuttling electrons through the RGO sheets; thus, the sandwich CdSe QDSCs exhibited an enhanced photovoltaic performance.[27] Another important and fundamental role of graphene is the scattering effect that resulted in enhancing the light adsorption capacity of the devices. A number of studies have demonstrated that graphene can be coupled with other noble metal or semiconductor materials, subsequently resulting in novel optical properties.[28−30] For example, Tripathi et al. reported that the Ag/Graphene composite thin-film can trap maximum normally incident light for photovoltaic applications with introduction of a graphene scattering effect, resulting in a 6.35% enhancement in J_{sc}.[28] Kamat et al. reported an RGO/CdSe nanocomposite improved photocurrent response and the charge separation in QDSCs.[29]

In this work, RGO was successfully introduced by immersion to a CdS/CdSe co-sensitized QDSCs system. The amount of RGO deposited on the QDs-sensitized TiO_2 films was regulated by controlling the immersing time in RGO dispersed ethanol solution. It was found that the introduction of RGO increased the absorbance of the sensitized photoanode in visible light due to the scattering effect, and thus, a large short-circuit current density. Although the QDs-sensitized TiO_2 films modified with RGO may have possibly accelerated the electron transmission, the defects in RGO would cause increased charge recombination. When the CdS/CdSe QDs co-sensitized TiO_2 film with 3 min RGO deposition was applied, the PCE of the resultant QDSCs was significantly improved compared with the solar cells without RGO deposition. A PCE up to 5.28% (V_{oc} = 572 mV, J_{sc} = 15.8 mA/cm^2) has been achieved with a RGO layer (3 min), an almost 13% enhancement compared to the solar cells without RGO.

2. EXPERIMENTAL SECTION

2.1. Chemicals and Materials. Titanium oxide (TiO_2, Degussa, P25), α-terpineol ($C_{10}H_8O$, 95%, Aladdin), ethyl cellulose (EC) ($[C_6H_7O_2(OC_2H_5)_3]_n$, 48.0−49.5% (w/w) as ethoxyl, Sigma-Aldrich), sodium sulfide anhydrate ($Na_2S\cdot 9H_2O$, ≥98.0%, Sigma-Aldrich), cadmium nitrate tetrahydrate ($Cd(NO_3)_2\cdot 4H_2O$, 98.0%, Sigma-Aldrich), nitrilotriacetic acid trisodium salt monohydrate ($N(CH_2COONa)_3$, ≥98.0%, Sigma-Aldrich), sodium sulfite anhydrous (Na_2SO_3, ≥98%, Aladdin), cadmium acetate dihydrate ($Cd(AC)_2\cdot 2H_2O$, 98.0%, Sigma-Aldrich), zinc nitrate hexahydrate($Zn(NO_3)_2\cdot 6H_2O$, 99.99%, Aladdin), selenium powder (Se, 200mesh, 99.999%, Alfa), sodium carbonate ($NaCO_3$, 99.5%, Aladdin), and sodium borohydride ($NaBH_4$, 98%, Aladdin) were all directly used without further purification. RGO is made in the laboratory. Ultrapure deionized water was used for the preparation of all aqueous solutions.

2.2. Preparation of Mesoporous TiO_2 Films. Mesoporous TiO_2 film was prepared as follows from the previously published literature.[17] A TiO_2 paste is composed with an amount of 0.5 g of commercial P25 nanoparticles mixed with 1.75 g of α-terpineol and 0.25 g of ethyl cellulose which was dispersed into 10.0 mL of ethanol in a round-bottom flask.

DOI: 10.1021/acs.jpcc.7b06192
J. Phys. Chem. C 2017, 121, 18430−18438

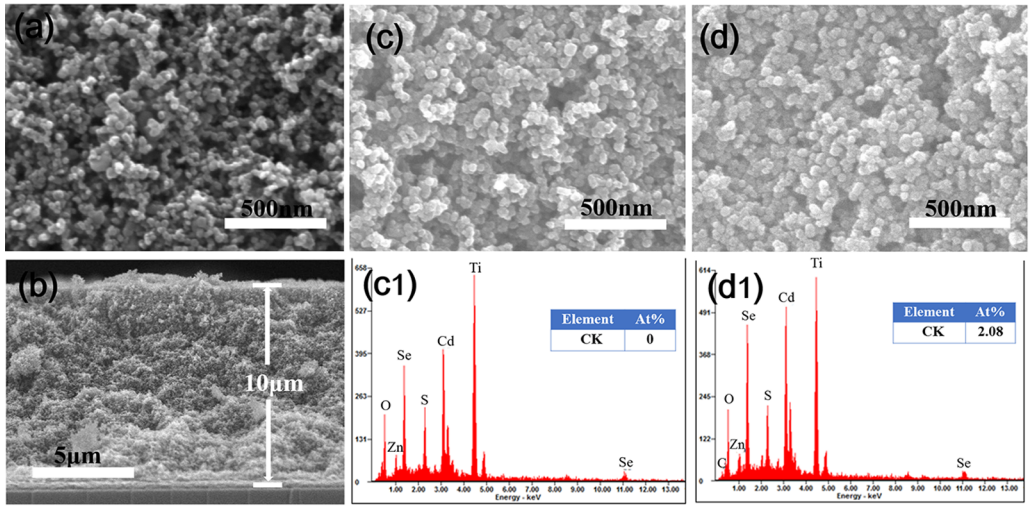

Figure 2. (a) Top view and (b) cross-sectional view SEM images of TiO_2 photoanode. (c, d) Top view SEM images and (c1, d1) EDX spectra of QDs-sensitized TiO_2 photoanodes without and with RGO (3 min), respectively.

Then, the TiO_2 colloidal solution, via stirring to remove the ethanol, formed the white TiO_2 paste. Subsequently, the white TiO_2 paste coated the clean FTO substrate via the doctor blading method; after then, it was sintered at 500 °C for 30 min in air.

2.3. Deposition of CdS/CdSe QDs and RGO Layer. CdS QDs and CdSe QDs were deposited on the surface of TiO_2 film by successive ionic layer adsorption and reaction (SILAR) and chemical bath deposition (CBD), respectively. The detailed experimental procedures were described in our previous paper.[17] The film was, respectively, immersed into a 0.1 M $Cd(NO_3)_2$ solution and 0.1 M solution for 1 min, after being rinsed with methanol and dried. After 5 such cycles, CdS QDs on the surface of TiO_2 film can be obtained. Then, the TiO_2/CdS film was immersed vertically in a solution containing 0.1 M Na_2SeSO_3, 0.1 M $Cd(CH_3COOH)_2{\cdot}2H_2O$, and 0.2 M $N(CH_2COONa)_3$ with a volume ratio of 1:1:1, under dark condition for 3 h at room temperature.

Graphene oxide (GO) was prepared by a modified Hummers method described in our previous work.[31] The RGO was obtained via a hydrothermal reduction treatment by the following procedure.[32] Briefly, an amount of 85 mg of GO was dispersed in ultrapure water with the solution concentration of 1.0 mg/mL, and adding Na_2CO_3 under ultrasonic for 3 h to adjust the pH value of 9−10. Subsequently, 0.8 g of $NaBH_4$ was dissolved in the as-prepared solution under vigorous stirring and reacted for 1 h under 80 °C, after cooling to room temperature and centrifugation to obtain RGO. The as-prepared RGO was dispersed in 250 mL of anhydrous ethanol via ultrasonic for 30 min and the QDs-sensitized TiO_2 films were coated with RGO by dipping in this transparent solution with different immersing times to control the amount of deposited RGO. The treatment using 0, 1, 3, and 5 min is abbreviated as TQ, TQR-1, TQR-3, and TQR-5 respectively.

ZnS passivation was deposited by a SILAR method. Briefly, the film was immersed in 0.1 M $Zn(NO_3)_2$ and in 0.1 M Na_2S for 1 min following each immersion, and this process was repeated for 2 times. Figure 1 illustrates explicitly the fabrication steps of the TQ photoanode deposited ZnS and RGO in different sequence. The TiO_2/CdS/CdSe film passivating with ZnS and then treated with RGO (3 min) was designated TQZR-3 and the TiO_2/CdS/CdSe film treated with RGO (3 min) first, and then deposited with ZnS layer was designated TQRZ-3, the TiO_2/CdS/CdSe/ZnS (designated TQZ) as a comparison.

2.4. Solar Cell Fabrication. The polysulfide electrolyte was composed of 1 M S and 1 M Na_2S in deionized water under 50 °C. A Cu_2S film on a brass foil was employed as counter electrode. The counter electrode was made by dipping in 37% HCl for 0.5 h under 80 °C and then rinsing with water and drying; subsequently, it was vulcanized for 20 min through the polysulfide electrolyte. The sandwich device was assembled using a Scotch tape spacer for measuring electrochemistry performance. The active area of the QDSCs was 0.196 cm^2.

2.5. Characterization. The morphology of the photoanode films was characterized by means of scanning electron microscopy (SEM, FEI Quanta 250) and transmission electron microscopy (TEM, Tecnai G2 F20). The elemental composition analysis of the samples was carried out by an energy dispersive X-ray spectroscope (EDX) integrated in SEM. The X-ray photoelectron spectra (XPS) were collected using a Thermo ESCALAB 250XI spectrometer. Light absorption properties of the sensitized photoanodes were studied using a UV−vis spectrophotometer (Hitachi U-3900H). Photovoltaic property parameters include open-circuit voltage (V_{oc}), short-circuit current density (J_{sc}), fill factor (FF), and PCE, and they were characterized by a Keithley 2400 source meter under a simulated AM 1.5 G sunlight with a power density of 100 mW/cm^{-2}. The incident photon-to-current conversion efficiency (IPCE) was carried out using a 7-SCSpec response measurement system. Electrochemical impedance spectroscopy (EIS) was obtained via an impedance analyzer (AUTOLAB PGSTAT302N) in the dark under the open-circuit voltage and frequency applied ranged from 0.1 to 100 K Hz. Intensity modulated photocurrent spectroscopy (IMPS) was measured on the same electrochemical workstation with a frequency response analyzer under an intensity-modulated (30−150 Wm^{-2}) light emitting diode (LED 470 nm) driven by a electrochemical workstation source supply. The frequency range was set from 10 kHz to 0.5 Hz for IMPS.

3. RESULTS AND DISCUSSION

Figure 2a,b shows the top view and cross-sectional view SEM images of TiO_2 mesoporous film, respectively. As seen from

DOI: 10.1021/acs.jpcc.7b06192
J. Phys. Chem. C 2017, 121, 18430−18438

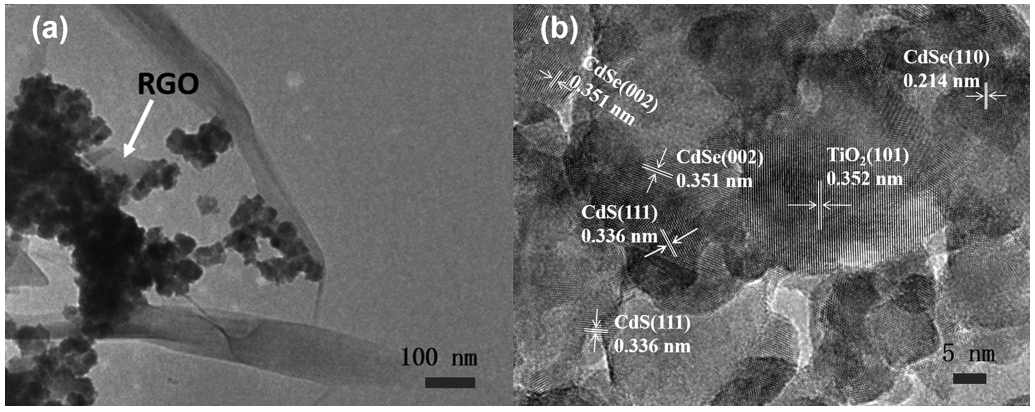

Figure 3. (a) TEM and (b) high-resolution TEM images of the TQZR-3 sample showing the presence of RGO, CdS and CdSe QDs, and TiO_2 nanocrystallites.

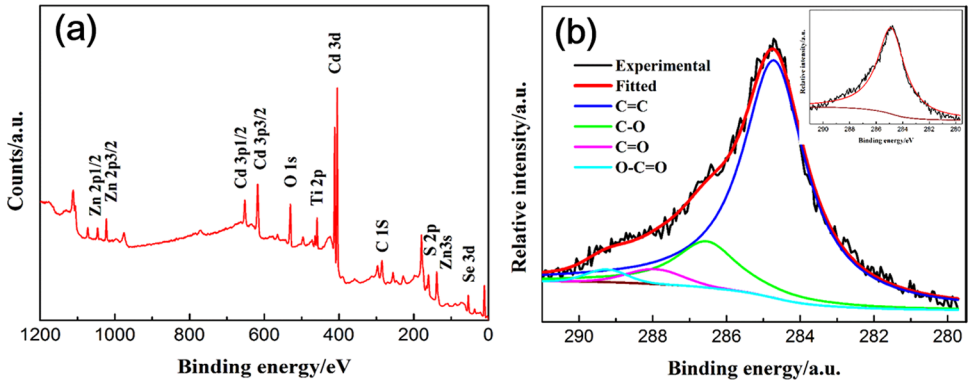

Figure 4. XPS of the TQZR-3 sample: (a) the full spectrum and (b) C 1s region (inset displays the C 1s of the TQZ sample).

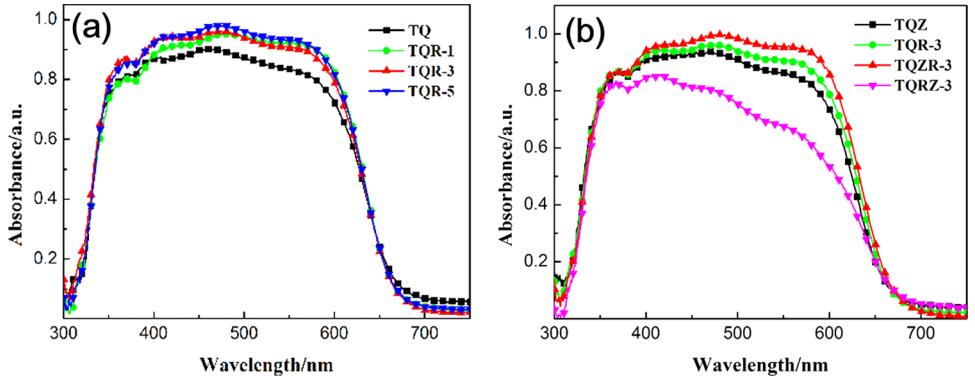

Figure 5. UV−visible light absorption spectra of (a) the QDs-sensitized TiO_2 films coated with RGO with different treating times (0, 1, 3, and 5 min) and (b) the TQR-3 sample passivating with different sequence of ZnS, the TQZ sample as a comparison.

SEM images, a typical morphology of a TiO_2 nanostructure is composed of nanoparticles with an average size of about 25 nm and a thickness of approximately 10 μm, indicating the porosity and thickness are much suitable for deposition of CdS or CdSe QDs to boost the performance of the TiO_2 photoanode.[33] Panels (c) and (d) in Figure 2 are the top view SEM images of CdS/CdSe/ZnS QDs-sensitized TiO_2 films without and with RGO (3 min), respectively. As displayed in Figure 2c,d, there is no apparent change in the surface morphology of QDs-sensitized TiO_2 film after RGO deposition; furthermore, the difference in surface morphology of samples is difficult to determine and inconclusive. It is also difficult to display RGO sheets in Figure 2d, which may be attributed to a less amount of RGO. The EDX spectra on the top of the QDs-sensitized TiO_2 film shown in Figure 2c1,d1 revealed the distribution of Ti, O, Cd, S, Se, and Zn elements in the film. The C element ratio was 2.08% in the TQZ coated RGO (3 min) (TQZR-3), indicating that less amount of RGO is present in the TQZR-3.

To further obtain the microscopic morphology and structure information, the TEM and HRTEM analyses of the TQZR-3 sample have been performed as displayed in Figure 3a,b. The TEM image in Figure 3a confirmed that thin RGO sheets were incorporated in the TQZR-3 sample. The HRTEM image revealed that the lattice spacing of 0.352 nm is the (101) plane of TiO_2. The lattice spacings of 0.336, 0.351, and 0.214 nm are

DOI: 10.1021/acs.jpcc.7b06192
J. Phys. Chem. C 2017, 121, 18430−18438

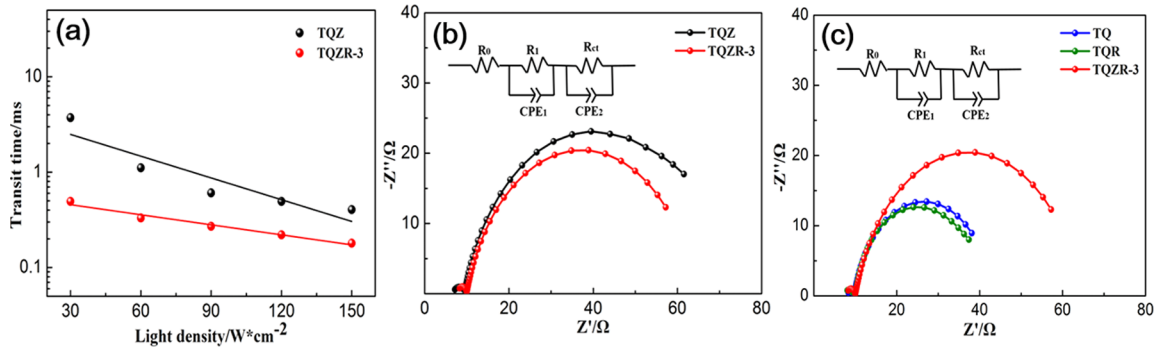

Figure 6. (a) Electron transit time measured by IMPS at different light densities. (b, c) Nyquist plots of EIS spectra measured under the open-circuit voltage (V_{oc}) at dark condition (insets display the corresponding equivalent circuit).

the (111) crystal plane of CdS QDs and (111), (110) crystal planes of CdSe QDs, respectively.

The chemical composition and the state of elements on the surface of the two samples were analyzed by XPS. All the data are corrected with respect to the standard peak of C 1s. As shown in Figure 4a, the total survey spectra showed the presence of Ti, O, Cd, S, Se, Zn, and C elements. To further demonstrate the existence of RGO on the surface of the TiO_2/QDs/ZnS film, the high resolution C 1s spectra of the TQZR-3 sample is shown in Figure 4b. It is clearly acknowledged that the abundance of various oxygen-containing functional groups on the surface of GO has been reported; the efficient reduction of GO to RGO via hydrothermal reduction treatment was confirmed by the C 1s spectrum.[32] Different with the high resolution C 1s spectra of the TQZ sample (inset in Figure 4b), the C 1s spectra of the TQZR-3 sample deconvoluted into four different states; the peaks located at 284.7, 286.5, 287.9, and 289.3 eV are corresponding to C═C, C-O, C═O, and O═C-O functional groups, respectively. Comparing with Martin's work,[32] in which we used the same GO reduction procedure, the binding energy positions and corresponding functional groups are matched well, indicating RGO has been successfully covered on the surface of TiO_2/QDs/ZnS.

Figure 5a illustrates the light absorbance spectra of sensitized film treated with RGO in different times. It is found that all the absorption onsets are around 610 nm, which is the typical band gap characteristic of CdSe QDs. In Figure 5a, the absorption edges of the QDs-sensitized TiO_2 films coated without or with RGO show almost no changes after modification with RGO. Similar to the result of a previous report, the unchanged absorption edges for the QDs-sensitized TiO_2 films coated with RGO may be ascribed to a linker-free connected RGO and CdSe.[30] As shown in Figure 5a, the absorbance of the QDs-sensitized TiO_2 films coated with RGO is much higher than that without RGO in the range of visible light. This was attributed to the scattering effect of RGO, which can be generally observed in RGO-based semiconductor composites.[28,30] It can be also found that, as the treating time of RGO increased systematically, the absorbance increased slightly as well, indicating the amount of RGO has a minor influence on the absorbance of the sensitized photoanodes. In order to get a synergetic effect between QDs and RGO, it is crucial to control the addition ratios of RGO, which leads to optimum photovoltaic performance. The dependence of average photovoltaic properties on RGO treating time is investigated by photocurrent density−voltage ($J-V$) test as shown in Figure S1, and the parameters of cell devices are summarized in Table S1. The champion cell exhibited an efficiency of 4.16%, and the highest value of J_{sc} is 15.1 mA/cm^2 for the cell with 3 min RGO treatment. It is worth mentioning that there is a typical increase in J_{sc} when increasing the loading amount of RGO (from 0 to 3 min), but further increasing the RGO amount decreased the J_{sc}. The reason will be explained in the later discussion. Hereafter, all the following investigation and discussion are based on the 3 min RGO treated sensitized photoanode.

As has been pointed out by Yang et al., the ZnS barrier layer covering on QDs-sensitized TiO_2 film can restrain recombination processes to improve the performance of the cell.[34] As reflected in Figure 5b, the absorbance of the TiO_2/CdS/CdSe passivating with ZnS and then treated with RGO (TQZR-3) is higher than that of the QDs without the ZnS layer. The high absorbance of the TQZR-3 sample might be ascribed to the ZnS passivation of the QD surface states which can prevent electron trapping.[35] For sample of TQRZ-3, which is the TiO_2/CdS/CdSe treated with RGO first, and then deposited with ZnS layer, exhibited a lower absorption intensity compared with other samples, especially weaker than the sample without RGO (TQZ). This may be attributed to the shielding effect of ZnS that caused the RGO surface to be densely covered by the ZnS component, leading to diminishing the scattering effect of RGO. Another explanation is that the interfacial interaction between ZnS and RGO might also contribute to the noticeable change of absorbance between TQZR-3 and TQRZ-3.[36,37] Apparently, there is a strong dependence between the photovoltaic performance and the deposition sequences of RGO. The $J-V$ curves and detailed corresponding average photovoltaic parameters of the solar cells with different sequences of RGO deposition are shown in Figure S2 and Table S2, respectively. The photovoltaic parameters of the sample TQRZ-3 matched the absorption profile well, in which reduction of absorbance resulting in poor performance compared with the other solar cells. Moreover, compared with TQR-3 of the multisensitizer system, the V_{oc} of TQZ is 602 mV, which is higher than that of TQR (494 mV). As mentioned above, the ZnS passivation layer can be reduced and prevented from the charge recombination process; the reduced interface charge recombination is often used to explain the higher V_{oc}.[38] Hereafter, the TQZR-3 cell is investigated as a model in the following discussion.

The effect of the RGO layer on the transport dynamics and recombination kinetics in QDSCs was investigated by means of intensity modulated photocurrent spectroscopy (IMPS) and electrochemical impedance spectroscopy (EIS), respectively.

DOI: 10.1021/acs.jpcc.7b06192
J. Phys. Chem. C 2017, 121, 18430−18438

The electron transport time (τ_d) could be estimated from the IMPS plots, according to the following expression[39]

$$\tau_d = \frac{1}{2\pi f_{IMPS}} \quad (1)$$

where the f_{IMPS} is the characteristic minimum frequency of the IMPS imagery component. As shown in Figure 6a, the IMPS results at varied light intensities clearly illustrate that for QDSCs based on TQZR-3 (0.49−0.18 ms) is shorter than that based on TQZ (3.73−0.40 ms). The shorter τ_d (faster transport rate) observed in RGO modified TiO_2/QDs/ZnS QDSCs is likely to attribute to the higher electron mobility of RGO, which is building a superhighway for fast electron diffusion.[40]

Figure 6b displays the Nyquist plots for the QDSCs analyzed under the open-circuit voltage (V_{oc}) at dark condition in the frequency range of 0.1 Hz to 100 kHz. QDSCs can be viewed as an equivalent circuit combining a series resistor with some parallel connected resistor and capacitor as illustrated in the inset of Figure 6b. In the Nyquist plot (Figure 6b), R_0 represents the charge transport resistance in FTO and the overall series resistances corresponding to the intercept of the horizontal ordinate, R_1 represents the charge transfer resistance at the counter electrode/electrolyte interface corresponding to the first small semicircle at high frequency, and R_{ct} corresponds to the charge transfer resistance at the TiO_2/QDs/electrolyte interfaces, respectively, which is denoted as the second large semicircle at intermediate frequency.[1,41] The fitting results of the EIS via Z-view software are shown in Table 1. The R_{ct} of the QDSCs are found to be 62.8 and 54.7 Ω for TQZ and TQZR-3 cells, respectively. It is well-known that R_{ct} represents the charge recombination resistance and the lower value of R_{ct} indicates the larger charge recombination occurring in the device interface.[42] The corresponding electron lifetime (τ_n) can be calculated from $\tau_n = C_\mu \times R_{ct}$, and the obtained τ_n values for TQZ and TQZR-3 cells are 158 and 135 ms, respectively.[43] Both the lower R_{ct} and the shorter τ_n of TQZR-3 QDSCs reveal the increased charge recombination after the RGO decoration in spite of the faster electron transport benefit from the superior electronic mobility of RGO.

Table 1. Fitting Results of the EIS of QDSCs

sample	R_0 (Ω)	R_1 (Ω)	R_{ct} (Ω)	C_μ (mF)	τ_n (ms)	ω_{max} (Hz)
TQZR-3	7.9	2.0	54.7	2.5	135	2.1
TQZ	7.5	1.9	62.8	2.5	158	1.7
TQR-3	7.7	2.1	34.6	2.4	84	5.4
TQ	7.8	1.9	36.3	2.6	96	3.4

To further better understand the impacts of RGO on charge recombination, the different sensitized photoanodes with and without ZnS passivation are also investigated by EIS test, which is shown in Figure 6c, and the fitting results of cell devices are also summarized in Table 1. It can be found that introduction of RGO to QDs-sensitized TiO_2 films may accelerate the recombination on the interface in QDSCs. The possible reason is attributed to the fact that the presence of defects of RGO can capture the photogenerated charge, leading to the severe recombination on the interface between QDs and RGO. An overview of the literature demonstrated that the reduction of GO inevitably contains residual small amounts of oxygenated functional groups and a particularly large population of defects, which results in considerable disruption of the 2D π-conjugation of the electronic structure of RGO.[44] Taking the more defects on RGO into consideration, the longer immersing times of the sample in RGO, the more severe charge recombination in RGO modified TiO_2/QDs QDSCs, which could explain the lower J_{sc} and V_{oc} for the TQR-5 cell as mentioned above. From Figure 6c and Table 1, the R_{ct} value for the QDSCs with the ZnS layer insertion is 54.7 Ω, while the R_{ct} for the QDSCs without the inserted passivation layer is only 34.6 Ω. The ZnS layer located between QDs and RGO behaves as an effective passivation layer which reduces the surface charge recombination.

Figure 7a shows the $J-V$ curves of the TiO_2/QDs/ZnS QDSCs with and without RGO modification measured under AM 1.5 simulated sunlight with a power density of 100 mW/cm^2. The main photovoltaic parameters of the two devices, such as J_{sc}, V_{oc}, FF, and PCE, are summarized in Table 2. The TQZR-3 cell generated a J_{sc} = 15.8 mA/cm^2, V_{oc} = 572 mV, FF = 0.59 and achieving a high PCE = 5.28%, higher than the efficiency of 4.69% without RGO.

Table 2. Photovoltaic Properties Obtained from the $J-V$ Curves of QDSCs Based on TQZ and TQZR-3

sample	V_{oc} (mV)	J_{sc} (mA/cm^2)	FF	PCE (%)
TQZ	602	13.7	0.57	4.69
TQZR-3	572	15.8	0.59	5.28

It is worth noting that the V_{oc} decreased with deposition of RGO in QDSCs. For QDSCs, it is generally considered that a decrease in the frequency at the maximum imaginary resistance of the second semicircle (ω_{max}) in the Nyquist plot is related to

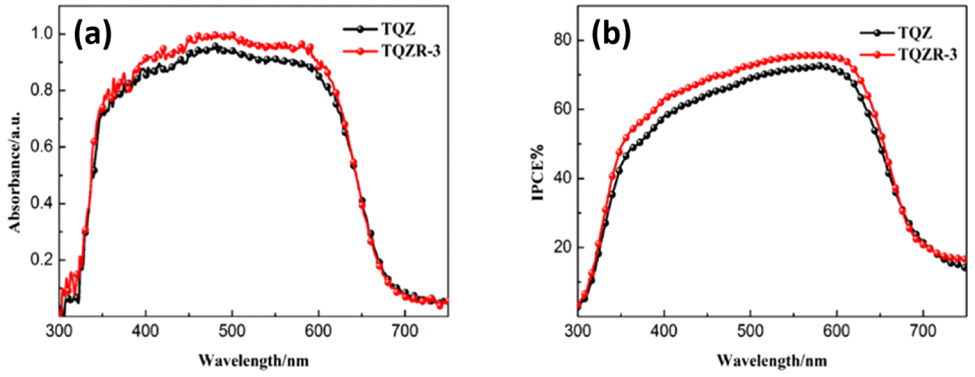

Figure 7. (a) $J-V$ curves and (b) IPCE spectra of QDSCs based on TQZ and TQZR-3.

DOI: 10.1021/acs.jpcc.7b06192
J. Phys. Chem. C 2017, 121, 18430−18438

an increase in V_{oc} due to the backward reaction at open-circuit conditions under illumination. The V_{oc} of a QDSC is calculated by the following equation[45,46]

$$V_{oc} = \frac{RT}{\beta F}\ln\left(\frac{AI}{n_0 k_b[S_n^{2-}] + n_0 k_r[h^+]}\right) \quad (2)$$

where R is the molar gas constant, T is the room temperature, F is the Faraday constant, and β is the reaction order for S_n^{2-} and electrons, A is the active area of the photoanode, I is the incident photon flux, n_0 is the concentration of accessible electronic states in the TiO_2 conduction band, and k_b and k_r are the kinetic constant of the back reaction of the injected electrons with S_n^{2-} and the recombination of these electrons with the hole (h^+), respectively. Obviously, considering the $RT/\beta F$ and AI are unchanged for the different devices, and the concentration of S_n^{2-} in the polysulfide electrolyte is constant under the measuring state. So $n_0 k_r [h^+]$ as the loss term can be neglected. The ω_{max} of the Nyquist plots is viewed as the back reaction constant, therefore, V_{oc} will logarithmically depend on $1/\omega_{max}$.[46,47] As shown in Table 1, the ω_{max} of TQZR-3 (2.1 Hz) is larger than that of the TQZ (1.7 Hz), the larger ω_{max} of TQZR-3 achieves in the small V_{oc}. Obviously, the increased charge recombination is the main reason for the reduced the V_{oc}, which corresponds to the conclusion of EIS.

J_{sc} under a particular light source is calculated by the following equation:[43]

$$J_{sc} = q\int_{\lambda_{min}}^{\lambda_{max}} \eta_{IPCE}\Phi_{ph}^{source}(\lambda)\,d\lambda \quad (3)$$

λ_{min} and λ_{max} are the wavelengths where the IPCE vanishes, and Φ_{ph}^{source} is the incident photon flux. Figure 7b shows IPCE spectra for the TiO_2/QDs/ZnS QDSCs with and without RGO in the range of wavelength from 300 to 800 nm. According to eq 3, the calculated J_{sc} values from the IPCE for the TQZ and TQZR-3 solar cells are 12.3 and 14.2 mA/cm^2, which is consistent with the values obtained from the $J-V$ curves under the error range. On the basis of the transport-limited recombination model developed by Frank et al.,[48] introduction of the RGO layer has a negligible effect on the charge collection despite that it accelerates the electron transport rate in QDSCs. As shown in Figure 5b, a significant enhancement in the IPCE can be seen for TQZR-3 cells with the highest IPCE of ~76% in the wavelength range of 400−600 nm. The overall photoresponse of the solar cell matches well with the absorption features, with the photocurrent onsets directly correlated with the absorption onsets. As stated in the discussion above, the enhanced IPCE is mainly ascribed to the increased light absorption by the RGO as surfaced-modification layer, which led to achieving the high J_{sc}.

4. CONCLUSIONS

Introduction of RGO to CdS/CdSe QDs co-sensitized TiO_2 films has been demonstrated to improve the power conversion efficiency of the QDSCs. Different immersion times and deposition sequences between ZnS and RGO have been found to affect the photovoltaic properties of the corresponding cells. UV−vis and IPCE showed that the introduction of RGO increased absorption of light due to the possible scattering effects, consequently generating more excitons, leading to an improved J_{sc}. The IMPS result suggests that introduction of RGO can accelerate the electronic transport rate in QDSCs, though it does not facilitate the improvement of solar cells performance. However, EIS revealed that the existential defects in RGO likely increase the possible charge recombination rate in QDSCs, leading to a reduced V_{oc}. When the ZnS passivation layers were deposited between QDs and RGO, the QDSCs with the best configuration, TiO_2/CdS/CdSe/ZnS/RGO (3 min), reached a PCE of 5.28%, J_{sc} of 15.8 mA/cm^2, and V_{oc} of 572 mV.

■ ASSOCIATED CONTENT

Supporting Information

The Supporting Information is available free of charge on the ACS Publications website at DOI: 10.1021/acs.jpcc.7b06192.

Optimized the deposited time of RGO based on the TiO_2/CdS/CdSe and the configuration structure of the solar cells, photovoltaic properties obtained from the $J-V$ curves such as J_{sc}, V_{oc}, FF, and PCE (PDF)

■ AUTHOR INFORMATION

Corresponding Authors

*E-mail: hjuan05@sina.com (J.H.).
*E-mail: gzcao@u.washington.edu (G.C.).

ORCID

Guozhong Cao: 0000-0003-1498-4517

Notes

The authors declare no competing financial interest.

■ ACKNOWLEDGMENTS

This work was supported by the National Natural Science Foundation of China (Nos. 51362026, 61376011).

■ REFERENCES

(1) Tian, J.; Zhang, Q.; Zhang, L.; Gao, R.; Shen, L.; Zhang, S.; Qu, X.; Cao, G. ZnO/TiO_2 Nanocable Structured Photoelectrodes for CdS/CdSe Quantum Dot Co-sensitized Solar Cells. *Nanoscale* **2013**, *5*, 936−943.

(2) González-Pedro, V.; Xu, X. Q.; Mora-Seró, I.; Bisquert, J. Modeling High-Efficiency Quantum Dot Sensitized Solar Cells. *ACS Nano* **2010**, *4*, 5783−5790.

(3) Kamat, P. V. Quantum Dot Solar Cells. Semiconductor Nanocrystals as Light Harvesters. *J. Phys. Chem. C* **2008**, *112*, 18737−18753.

(4) Yu, Z.; Sandhu, S.; Fan, S. Efficiency Above the Shockley-Queisser Limit by Using Nanophotonic Effects to Create Multiple Effective Bandgaps with a Single Semiconductor. *Nano Lett.* **2014**, *14*, 66−70.

(5) Hanna, M. C.; Nozik, A. J. Solar Conversion Efficiency of Photovoltaic and Photoelectrolysis Cells with Carrier Multiplication Absorbers. *J. Appl. Phys.* **2006**, *100*, 074510.

(6) Du, J.; Du, Z.; Hu, J. S.; Pan, Z.; Shen, Q.; Sun, J.; Long, D.; Dong, H.; Sun, L.; Zhong, X.; Wan, L. J. Zn-Cu-In-Se Quantum Dot Solar Cells with a Certified Power Conversion Efficiency of 11.6%. *J. Am. Chem. Soc.* **2016**, *138*, 4201−4209.

(7) Mathew, S.; Yella, A.; Gao, P.; Humphry-Baker, R.; Curchod, B. F.; Ashari-Astani, N.; Tavernelli, I.; Rothlisberger, U.; Nazeeruddin, M. K.; Gratzel, M. Dye-sensitized Solar Cells with 13% Efficiency Achieved Through the Molecular Engineering of Porphyrin Sensitizers. *Nat. Chem.* **2014**, *6*, 242−247.

(8) NREL record solar cell effciency table. http://www.nrel.gov/ncpv/images/effciency_chart.jpg (accessed April, 2016).

(9) Lee, Y. S.; Gopi, C. V. V. M.; Venkata-Haritha, M.; Kim, H. J. Recombination Control in High-performance Quantum Dot-sensitized Solar Cells with a Novel TiO_2/ZnS/CdS/ZnS Heterostructure. *Dalton Trans.* **2016**, *45*, 12914−12923.

DOI: 10.1021/acs.jpcc.7b06192
J. Phys. Chem. C 2017, 121, 18430−18438

(10) Bai, H.; Wang, S.; Li, B.; Cao, G.; Tian, J.; Shen, T. Controlled Growth of Cu_3Se_2 Nanosheets Array Counter Electrode for Quantum Dots Sensitized Solar Cell Through Ion Exchange. *Sci. China Mater.* **2017**, *60*, 637−645.
(11) Zhou, R.; Wan, L.; Niu, H.; Yang, L.; Mao, X.; Zhang, Q.; Miao, S.; Xu, J.; Cao, G. Tailoring Band Structure of Ternary CdS_xSe_{1-x} Quantum Dots for Highly Efficient Sensitized Solar Cell. *Sol. Energy Mater. Sol. Cells* **2016**, *155*, 20−29.
(12) Kim, J.; Choi, H.; Nahm, C.; Moon, J.; Kim, C.; Nam, S.; Jung, D. R.; Park, B. The Effect of a Blocking Layer on the Photovoltaic Performance in CdS Quantum-Dot- Sensitized Solar Cell. *J. Power Sources* **2011**, *196*, 10526−10531.
(13) Lee, H. J.; Yum, J. H.; Leventis, H. C.; Zakeeruddin, S. M.; Haque, S. A.; Chen, P.; Seok, S. I.; Grätzel, M.; Nazeeruddin, Md. K. CdSe Quantum Dot-Sensitized Solar Cells Exceeding Efficiency 1% at Full-Sun Intensity. *J. Phys. Chem. C* **2008**, *112*, 11600−11608.
(14) Wang, G.; Wei, H.; Luo, Y.; Wu, H.; Li, D.; Zhong, X.; Meng, Q. A Strategy to Boost the Cell Performance of $CdSe_xTe_{1-x}$ Quantum Dots Sensitized Solar Cells Over 8% by Introducing Mn Modified CdSe Coating Layer. *J. Power Sources* **2016**, *302*, 266−273.
(15) Xu, X.; Wan, Q.; Luan, C.; Mei, F.; Zhao, Q.; An, P.; Liang, Z.; Xu, G.; Zapien, J. A. Fabrication of $CuInS_2$-sensitized Solar Cell via an Improved SILAR Process and Its Interface Electron Recombination. *ACS Appl. Mater. Interfaces* **2013**, *5*, 10605−10613.
(16) Tian, J.; Gao, R.; Zhang, Q.; Zhang, S.; Li, Y.; Lan, J.; Qu, X.; Cao, G. Enhanced Performance of CdS/CdSe Quantum Dot Cosensitized Solar Cells via Homogeneous Distribution of Quantum Dots in TiO_2 Film. *J. Phys. Chem. C* **2012**, *116*, 18655−18662.
(17) Huang, F.; Hou, J.; Zhang, Q.; Wang, Y.; Massé, R. C.; Peng, S.; Wang, H.; Liu, J.; Cao, G. Doubling the Power Conversion Efficiency in CdS/CdSe Quantum Dots Sensitized Solar Cells with a ZnSe Passivation Layer. *Nano Energy* **2016**, *26*, 114−122.
(18) Zhao, H.; Wu, Q.; Hou, J.; Cao, H.; Jing, Q.; Wu, R.; Liu, Z. Enhanced Light Harvesting and Electron Collection in Quantum Dots Sensitized Solar Cells by TiO_2 Passivation on ZnO Nanorod Arrays. *Science China Mater.* **2017**, *60*, 239−250.
(19) Shen, T.; Tian, J.; Li, B.; Cao, G. Ultrathin ALD Coating on TiO_2 Photoanodes with Enhanced Quantum Dot Loading and Charge Collection in Quantum Dots Sensitized Solar Cells. *Science China Mater.* **2016**, *59*, 833−841.
(20) Huang, F.; Zhang, L.; Zhang, Q.; Hou, J.; Wang, H.; Wang, H.; Peng, S.; Liu, J.; Cao, G. High Efficiency CdS/CdSe Quantum Dot Sensitized Solar Cells with Two ZnSe Layers. *ACS Appl. Mater. Interfaces* **2016**, *8*, 34482−34489.
(21) Hou, J.; Zhao, H.; Huang, F.; Jing, Q.; Cao, H.; Wu, Q.; Peng, S.; Cao, G. High Performance of Mn-doped CdSe Quantum Dot Sensitized Solar Cells Based on the Vertical ZnO Nanorod Arrays. *J. Power Sources* **2016**, *325*, 438−445.
(22) Cheng, K.; Meng, J.; Zhao, Y.; Wang, X.; Du, Z.; Wu, Y. Plasmon-enhanced Photocurrent Generation in Quantum Dot Sensitized Solar Cells by Coupling of Gold Nanocrystals. *Sci. Bull.* **2015**, *60*, 541−548.
(23) Jang, Y. H.; Jang, Y. J.; Kim, S.; Quan, L. N.; Chung, K.; Kim, D. H. Plasmonic Solar Cells: From Rational Design to Mechanism Overview. *Chem. Rev.* **2016**, *116*, 14982−15034.
(24) Novoselov, K. S.; Geim, A. K.; Morozov, S. V.; Jiang, D.; Zhang, Y.; Dubonos, S. V.; Grigorieva, I. V.; Firsov, A. A. Electric Field Effect in Atomically Thin Carbon Films. *Science* **2004**, *306*, 666−669.
(25) Bolotin, K. I.; Sikes, K. J.; Jiang, Z.; Klima, M.; Fudenberg, G.; Hone, J.; Kim, P.; Stormer, H. L. Ultrahigh Electron Mobility in Suspended Graphene. *Solid State Commun.* **2008**, *146*, 351−355.
(26) Chen, J.; Li, C.; Eda, G.; Zhang, Y.; Lei, W.; Chhowalla, M.; Milne, W. I.; Deng, W. Q. Incorporation of Graphene in Quantum Dot Sensitized Solar Cells Based on ZnO Nanorods. *Chem. Commun.* **2011**, *47*, 6084.
(27) Radich, J. G.; Dwyer, R.; Kamat, P. V. Cu_2S Reduced Graphene Oxide Composite for High-Efficiency Quantum Dot Solar Cells. Overcoming the Redox Limitations of S^{2-}/S_n^{2-} at the Counter Electrode. *J. Phys. Chem. Lett.* **2011**, *2*, 2453−2460.
(28) Kanade, P.; Yadav, P.; Kumar, M.; Tripathi, B. Plasmon-Induced Photon Manipulation by Ag Nanoparticle-Coupled Graphene Thin-Film: Light Trapping for Photovoltaics. *Plasmonics* **2015**, *10*, 157−164.
(29) Lightcap, I. V.; Kamat, P. V. Fortification of CdSe Quantum Dots with Graphene Oxide. Excited State Interactions and Light Energy Conversion. *J. Am. Chem. Soc.* **2012**, *134*, 7109−7116.
(30) Lin, Y.; Chen, W.; Liu, Y.; Geng, Z.; Zeng, J.; Pan, N.; Yan, L.; Wang, X.; Hou, J. G.; Zhang, K. Dramatically Enhanced Photoresponse of Reduced Graphene Oxide with Linker Free Anchored CdSe Nanoparticles. *ACS Nano* **2010**, *4*, 3033−3038.
(31) Hou, J.; Wu, R.; Zhao, P.; Chang, A.; Ji, G.; Gao, B.; Zhao, Q. Graphene−TiO_2(B) Nanowires Composite Material: Synthesis, Characterization and Application in Lithium-ion Batteries. *Mater. Lett.* **2013**, *100*, 173−176.
(32) Ambrosi, A.; Chua, C. K.; Bonanni, A.; Pumera, M. Lithium Aluminum Hydride as Reducing Agent for Chemically Reduced Graphene Oxides. *Chem. Mater.* **2012**, *24*, 2292−2298.
(33) Gratzel, M. Solar Energy Conversion by Dye-Sensitized Photovoltaic Cells. *Inorg. Chem.* **2005**, *44*, 6841−6851.
(34) Yang, S.-m.; Huang, C.-h.; Zhai, J.; Wang, Z.-s.; Jiang, L. High Photostability and Quantum Yield of Nanoporous TiO_2 Thin Film Electrodes Co-sensitized with Capped Sulfides. *J. Mater. Chem.* **2002**, *12*, 1459−1464.
(35) Guijarro, N.; Campina, J. M.; Shen, Q.; Toyoda, T.; Lana-Villarreal, T.; Gomez, R. Uncovering the Role of the ZnS Treatment in the Performance of Quantum Dot Sensitized Solar Cells. *Phys. Chem. Chem. Phys.* **2011**, *13*, 12024−12032.
(36) Kashinath, L.; Namratha, K.; Srikantaswamy, S.; Vinu, A.; Byrappa, K. Microwave Treated Sol−gel Synthesis and Characterization of Hybrid ZnS−RGO Composites for Efficient Photodegradation of Dyes. *New J. Chem.* **2017**, *4*, 1723−1735.
(37) Zhang, Y. H.; Zhang, N.; Tang, Z. R.; Xu, Y. J. Graphene Transforms Wide Band Gap ZnS to a Visible Light Photocatalyst. The New Role of Graphene as a Macromolecular Photosensitizer. *ACS Nano* **2012**, *6*, 9777−9789.
(38) Tian, J.; Uchaker, E.; Zhang, Q.; Cao, G. Hierarchically Structured ZnO Nanorods−Nanosheets for Improved Quantum Dot Sensitized Solar Cells. *ACS Appl. Mater. Interfaces* **2014**, *6*, 4466−4472.
(39) Fei, C.; Tian, J.; Wang, Y.; Liu, X.; Lv, L.; Zhao, Z.; Cao, G. Improved Charge Generation and Collection in Dye-sensitized Solar Cells with Modified Photoanode Surface. *Nano Energy* **2014**, *10*, 353−362.
(40) Xu, Y. F.; Wu, W. Q.; Rao, H. S.; Chen, H. Y.; Kuang, D. B.; Su, C. Y. CdS/CdSe Co-sensitized TiO_2 Nanowire-coated Hollow Spheres Exceeding 6% Photovoltaic Performance. *Nano Energy* **2015**, *11*, 621−630.
(41) Zhao, L.; Zhong, C.; Wang, Y.; Wang, S.; Dong, B.; Wan, L. Ag Nanoparticle-decorated 3D Flower-like TiO_2 Hierarchical Microstructures Composed of Ultrathin Nanosheets and Enhanced Photoelectrical Conversion Properties in Dye-sensitized Solar Cells. *J. Power Sources* **2015**, *292*, 49−57.
(42) Jiao, S.; Wang, J.; Shen, Q.; Li, Y.; Zhong, X. Surface Engineering of PbS Quantum Dot Sensitized Solar Cells with a Conversion Efficiency Exceeding 7%. *J. Mater. Chem. A* **2016**, *4*, 7214−7221.
(43) Zhao, H.; Huang, F.; Hou, J.; Liu, Z.; Wu, Q.; Cao, H.; Jing, Q.; Peng, S.; Cao, G. Efficiency Enhancement of Quantum Dot Sensitized TiO_2/ZnO Nanorod Arrays Solar Cells by Plasmonic Ag Nanoparticles. *ACS Appl. Mater. Interfaces* **2016**, *8*, 26675−26682.
(44) Zhang, N.; Yang, M. Q.; Liu, S.; Sun, Y.; Xu, Y. J. Waltzing with the Versatile Platform of Graphene to Synthesize Composite Photocatalysts. *Chem. Rev.* **2015**, *115*, 10307−10377.
(45) Wang, Q.; Moser, J.-E.; Grätzel, M. Electrochemical Impedance Spectroscopic Analysis of Dye-Sensitized Solar Cells. *J. Phys. Chem. B* **2005**, *109*, 14945−14953.
(46) Zhou, R.; Zhang, Q.; Uchaker, E.; Yang, L.; Yin, N.; Chen, Y.; Yin, M.; Cao, G. Photoanodes with Mesoporous TiO_2 Beads and Nanoparticles for Enhanced Performance of CdS/CdSe Quantum Dot Co-sensitized Solar Cells. *Electrochim. Acta* **2014**, *135*, 284−292.

DOI: 10.1021/acs.jpcc.7b06192
J. Phys. Chem. C 2017, 121, 18430−18438

(47) Lee, K.; Park, S. W.; Ko, M. J.; Kim, K.; Park, N. G. Selective Positioning of Organic Dyes in a Mesoporous Inorganic Oxide Film. *Nat. Mater.* **2009**, *8*, 665−671.
(48) Kopidakis, N.; Benkstein, K. D.; van de Lagemaat, J.; Frank, A. J. Transport-Limited Recombination of Photocarriers in Dye-Sensitized Nanocrystalline TiO_2 Solar Cells. *J. Phys. Chem. B* **2003**, *107*, 11307−11315.

DOI: 10.1021/acs.jpcc.7b06192
J. Phys. Chem. C 2017, 121, 18430−18438